The Effect of Propylene–Ethylene Copolymers with Different Comonomer Content on Melting and Crystallization Behavior of Polypropylene

Jinyao Chen, Ya Cao, Huilin Li

State Key Laboratory of Polymer Materials Engineering, Polymer Research Institute of Sichuan University, Chengdu 610065, People's Republic of China

Received 24 June 2009; accepted 23 October 2009
DOI 10.1002/app.31658
Published online 17 December 2009 in Wiley InterScience (www.interscience.wiley.com).

ABSTRACT: The effect of propylene–ethylene copolymers (PEc) with different ethylene-unit contents on melting and crystallization behaviors of isotactic-polypropylene (iPP) were investigated by differential scanning calorimetry (DSC) and polarized light microscopy (PLM). The results show that the addition of PEc decreases significantly crystallization temperature (T_c) of iPP, but slightly affects melting temperature (T_m). With increasing the ethylene-unit content of the propylene–ethylene copolymers, the decrease in crystallization temperature of iPP is smaller. The PLM results show that the spherulite growth rate decreases with increasing crystallization temperature for iPP and iPP/PEc blends. The higher the ethylene-unit content of the copolymers is, the lower the spherulite growth rate (G) of iPP/PEc blends is. The influence of the PEc on nucleation rate constant (K_g) and fold surface energy (σ_e) of iPP was examined by nucleation theory of Hoffman and Lauritzen. The results show that both K_g and σ_e of iPP/PE20(80/20) and iPP/PE23(80/20) blends are higher than those of iPP, demonstrating that the overall crystallization rate of iPP/PEc blends decreased as compared to that of iPP, resulting from the decrease of the nucleation rate and the spherulite growth rate of iPP. © 2009 Wiley Periodicals, Inc. J Appl Polym Sci 116: 1172–1183, 2010

Key words: polypropylene (PP); copolymer; blends; crystallization; nucleation theory

INTRODUCTION

The development of polymer blends has received much attention for many decades, driven mainly by the enhancements in their combined properties. The physical properties of polymer blends strongly depend not only on the miscibility between the components but also on their morphology and crystallinity.[1–10] The addition of the second component intensively influences on the crystal structures (including crystallinity, crystalline form and size, etc.) and the crystallization behaviors of the blends, finally on the mechanical properties in the solid state. Therefore, the blends that incorporate one or more crystallizable constituents have received continuing attentions because not only crystalline polymers are of considerable commercial importance but also blending crystalline polymers offers an effective route to novel structure–property relationships.[11–15]

Isotactic polypropylene (iPP) is a typical semicrystalline polymer with excellent combined properties. The iPP resins have been extensively used in automobile parts, household appliances, furniture, and construction industry. The crystallization behaviors and crystal morphologies of iPP are influenced by many factors, such as temperature gradients, shearing force, and additives. In addition, the difference in the crystallization behavior has a strong effect on the morphology and property in the solid state. The crystallization behaviors and morphologies of iPP blends were extensively investigated in the last decade.[16–28] In particular, binary blends of iPP and ethylene-propylene (EP) copolymers have been extensively studied from the commercial point of view.[29–39] According to the researches by Nitta and coworkers,[40–43] the EP copolymers with a propylene content of more than 84 mol % were miscible with iPP, in which the crystallizable propylene sequences in these EP copolymers were incorporated in crystal lattice of iPP and the other portions in the EP chains were excluded to the amorphous phases. The addition of the EP copolymers did not affect lamellar strength or crystalline morphology, but influence on the crystallization behaviors of the blends and decrease the crystallization rate of iPP. Lee and coworkers[44] reported liquid–liquid phase separation and its effect on crystallization in the extruded polypropylene/ethylene–propylene–rubber blends and found that the crystallization rate decreased with increasing liquid–liquid phase-separated time at

Correspondence to: H. Li (nic7703@scu.edu.cn).
Contract grant sponsor: National Basic Research Program of China; contract grant number: 2005CB623800.

190°C. Coppola and Greco[45] found a very close correlation between crystallization condition and mechanical property in a PP/EPR blend. The formation of the crystalline structure relates to liquid–liquid phase separation when the blend has an immiscibility gap, i.e., upper critical solution temperature (UCST)/lower critical solution temperature (LCST).

Many researches have been developed on the crystalline morphology and crystallization behavior of iPP blends, including iPP/EPDM, iPP/aPP, and iPP/sPP, etc.,[46–50] Keith and Padden[51,52] reported the effect of aPP on the crystallization behavior of the pure iPP. They found that with increasing aPP content in the iPP/aPP blends, a more open spherulitic texture was observed due to the incorporation of aPP diluent in the interfibrillar regions. The aPP component was reported to be miscible with iPP in the molten state from the evaluation of an equation of state theory using low molecular weight aPP.

The compatibility between iPP and different types of EP copolymers in the molten state was also inferred from thermal and morphological studies of the solid blends. Therefore, we find the need to know more information on the compatibility and its effect on the crystallization which may result in control of physical properties of the PP/EP copolymers blends. In the present work, we attempt to correlate the isothermal crystallization and melting behavior of iPP blends with propylene–ethylene copolymer (PEc) having the different ethylene-unit content (5–15 mol %) but similar molecular weight. These propylene–ethylene copolymers prepared with metallocene catalysts in combination with Dow's proprietary INSITE™ Technology and Solution Process exhibit relatively narrow molecular weight distribution and well-define microstructures, resulting in improving thermal performances and excellent physical properties as compared with the other metallocene catalyst-based products of comparable olefin content. In this article, the melting behaviors and isothermal crystallization kinetics of iPP/PEc blends are investigated by DSC and PLM. The dependence of thermal properties and crystallization morphology of iPP blends on both the ethylene-unit content and isothermal crystallization temperature are also discussed. The present work is part of a broad project related to the development of high impact resistance and high modulus materials based on iPP and the influence of different parameters on these properties.

EXPERIMENTAL

Materials

The propylene–ethylene random copolymers (VERSIFY™, PEc) used in the present study were kindly supplied by Dow Chemical (TX). The structure and property parameters of copolymers are summarized in Table I. iPP resins (F401) were supplied by Langang Chemical (Lanzhou, China) with melt flow rate = 2.5 g/10 min (230°C, 2.16 Kg).

TABLE I
Structure Parameters of Propylene–Ethylene Copolymers

Samples	Ethylene unit content (mol %)	Density (g/cm^3)	Melt flow rate (g/10 min)
PE20	5	0.888	2
PE22	9	0.876	2
PE23	12	0.866	2
PE24	15	0.858	2
PE30	5	0.888	8
PE32	9	0.876	8
PE33	12	0.866	8
PE34	15	0.858	8

Blends preparation

iPP pellets were mixed with the various amount of the copolymers, then extruded by using a counter-rotating twin-screw extruder (SHJ-20, Nanjing JNT, China) in which temperature profile was 180–195–195–190°C and screw velocity was 200 rpm. The extrudates were cut into pellets and then the pellets were compression molded into plaques with 1 mm thickness by using a compression-molding machine. The temperature was 190°C and the molded pressure was 15 MPa. The samples sandwiched between the stainless steels were heated at 190°C for 5 min to ensure complete melting under minimal pressure, followed for 10 min with 15 MPa and then cooled to room temperature for further analysis.

Dynamic mechanical thermal analysis

Dynamic mechanical thermal analysis (DMTA) was performed on a TA Q800 DMA operating in the tensile mode with specimens cut from the plaques. The relaxation spectrum was scanned from −70°C to 70°C with a frequency of 1 Hz and the heating rate of 3°C/min.

Differential scanning calorimetry

The thermal behaviors of the samples were carried out in a NETZSCH DSC 204 (Germany) differential scanning calorimeter. The samples of 5 mg sealed in aluminum pans, which were cut from the plaques, were heated rapidly and held at 200°C for 5 min to eliminate the heat history. Subsequently, the samples were cooled to 0°C at a rate of 10°C/min and held at 0°C for 5 min. Then, they were heated from 0°C to 200°C at a rate of 10°C/min. Crystallization and

melting temperature were obtained from the cooling and the second-heating thermograms, respectively.

Percent crystallinity of the iPP components in the blends was calculated by using the formula $X\% = H_f/H_0 \times 100$, where X is the degree of crystallinity, H_f is the heat of fusion of PP component, and H_0 is the heat fusion of the completely crystalline polymer, which is equal to 209 J/g for iPP.

Polarized light microscopy

The growth rate of spherulite radius was quantitatively investigated using an optical Polarized Light Microscopy (LEITZ LABORLUX 12POLS, Germany). The radius of a spherulite was measured as a function of time under the isothermal crystallization condition. For supplementary observations of the crystallization behavior, the microscopy was equipped with a hot stage. The hot stage could be held at a steady temperature to ±0.5 K by a proportional controller. In this experiment, the blend films obtained from pellets were sandwiched between a microscope slide and a cover glass, heated up to 200°C at a rate of 80°C/min and held at this temperature for 5 min to eliminate completely the heat history. Then, the films were quickly quenched to the given crystallization temperature at a rate of 80°C/min and allowed to crystallize isothermally.

For the growth rate determination, the radii of the growing spherulites were measured as a function of crystallization time. These measurements were conducted on at least three spherulites per crystallization temperature. Linear growth rates were obtained as the slope of the plot of the average spherulite radius versus time using the least square method. The data of the linear growth rate were further analyzed using the secondary nucleation theory of Lauritzen and Hoffman.

RESULTS AND DISCUSSIONS

Miscibility of iPP/PEc blends

The miscibility of iPP/PEc blends could be verified by DMTA measurements. The variation of Tan δ for iPP, iPP/PE20, iPP/PE22, iPP/PE23, and PP/PE24 blends with temperature is shown in Figure 1. The results from the DMTA show that iPP/PE20(80/20) and iPP/PE22(80/20) blends exhibit a single glass transition temperature (T_g), indicating that there is the good compatibility of iPP/PE20 and iPP/PE22 blends; while both iPP/PE23(80/20) and iPP/PE20(80/20) blends exhibit two individual glass transition temperature (T_g) of the component polymers, as expected of an immiscible polymer blend system. With increasing the ethylene-unit content of copolymers, the miscibility and interaction between iPP and PEc becomes worse. The difference in the miscibility of iPP/PEc blends will have different influence on the thermal and crystallization behaviors of the blends.

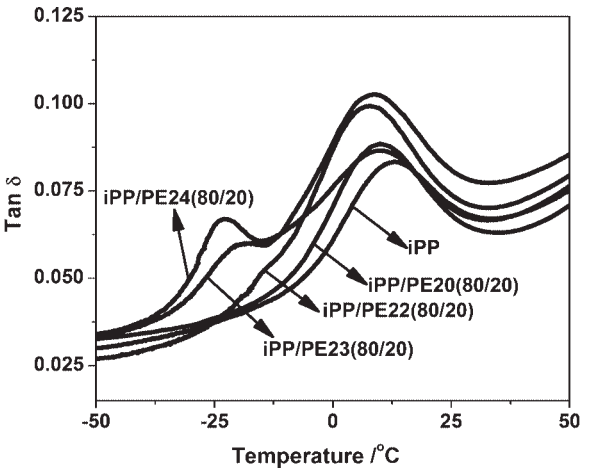

Figure 1 Temperature dependence of tan δ for iPP, iPP/PE20, iPP/PE22, iPP/PE23, and iPP/PE24 blends.

Thermal and crystallization behaviors of iPP/PEc blends

Figure 2(a,c) show the melting behaviors of iPP and iPP/PEc(80/20) blends, while Figure 2(b,d) show their crystallization behaviors. The heating curve of iPP revealed a sharp melting peak at a temperature T_m of 166.8°C with a melting enthalpy ΔH_f of 95 J/g. The cooling curve showed a sharp crystallization peak at a temperature T_c of 118.9°C with a crystallization enthalpy ΔH_c of 112 J/g. The melting temperatures and endothermic peaks of the iPP/PEc blends were almost in accordance with those of the iPP, indicating that the addition of PEc have little influence on the melting point of iPP. With the addition of PEc, the crystallization peak of iPP shifts to the lower temperature, indicating that the crystallization temperature of the iPP/PEc blends decreases. For the iPP/PE20 blend, the crystallization temperature decreases from 118.9°C of the pure iPP to 114.1°C. As can be seen from Figure 2, with the increase of ethylene-unit content in the propylene–ethylene copolymers, the decrease in the crystallization temperature for the iPP/PEc blends becomes smaller. This may be related to the compatibility between iPP and PEc. Because the copolymers with high ethylene-unit content are more immiscible with iPP than those with low ethylene-unit content, they have much weaker impact on the crystallization behaviors of iPP. On the other hand, with the decrease of the molecular weight in the propylene–ethylene copolymers, the crystallization temperature of iPP/PEc blends reduces more obviously, as showed in Figure 2(d). Comparing Figure 2(a–c), the change of

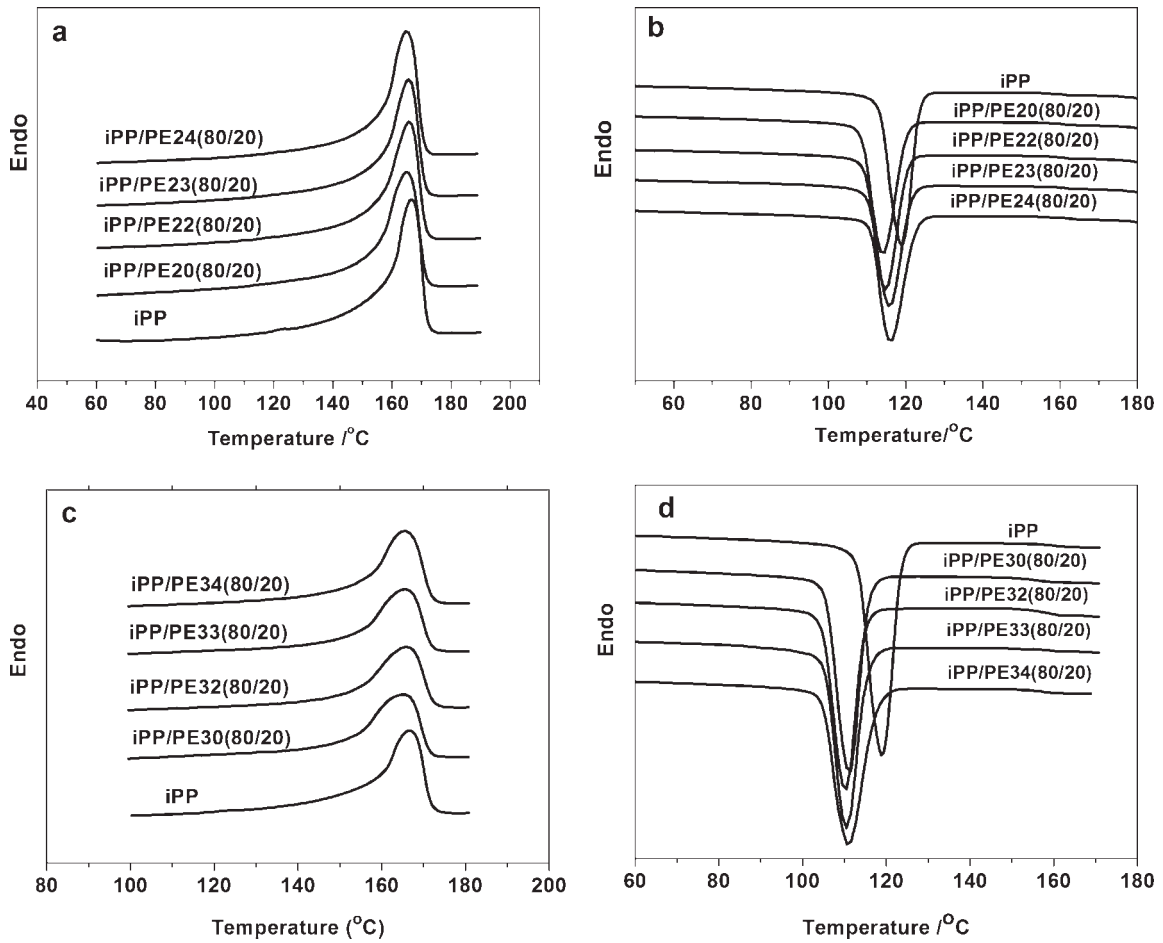

Figure 2 DSC curves of iPP blends with the copolymers. (a) and (c) heating scans; (b) and (d) cooling scans.

molecular weight in PEc has little influence on the melting temperature of iPP, but it has greater influence on the crystallization temperature.

Table II summarizes the melting and crystallization parameters of iPP/PEc blends obtained from DSC curves. ($T_{onset} - T_c$) is a measure of overall rate of crystallization of the system, which decreases with the increase of the crystallization rate. It can be found from Table II that with the addition of the PEc copolymers, ($T_{onset} - T_c$) of the iPP/PEc blends increases, indicating that the overall crystallization rate of the blends decreases. With the increase of ethylene comonomer content in the propylene–ethylene copolymers, the value of ($T_{onset} - T_c$) of the iPP/PEc blends reduces. This may be due to the fact that higher the ethylene comonomer content in the propylene–ethylene copolymers is, the worse the miscibility and interaction between the copolymers and iPP is, which leading to the weaker impact on the crystallization behavior of iPP.

TABLE II
The Crystallization and Melting Parameters of iPP/PEc (80/20) Blends from DSC Curves

Samples	$\Delta H_{f,PP}$ (J/g)	X_c of iPP (DSC)%	T_m (°C)	T_c (°C)	T_{onset} (°C)	$T_{onset} - T_c$ (°C)
iPP	95	45.5	166.8	118.9	123.6	4.7
iPP/PE20	85	50.8	165.1	114.1	120.1	6.0
iPP/PE22	83	49.6	165.9	114.7	120.3	5.6
iPP/PE23	79	47.2	165.7	115.8	121.4	5.6
iPP/PE24	68	40.7	165.2	116.4	121.5	5.1
iPP/PE30	80	47.8	165.3	110.5	115.6	5.1
iPP/PE32	77	46.1	166.1	110.2	115.2	5.0
iPP/PE33	76	45.5	165.6	110.4	115.4	5.0
iPP/PE34	70	41.9	165.8	110.8	115.6	4.8

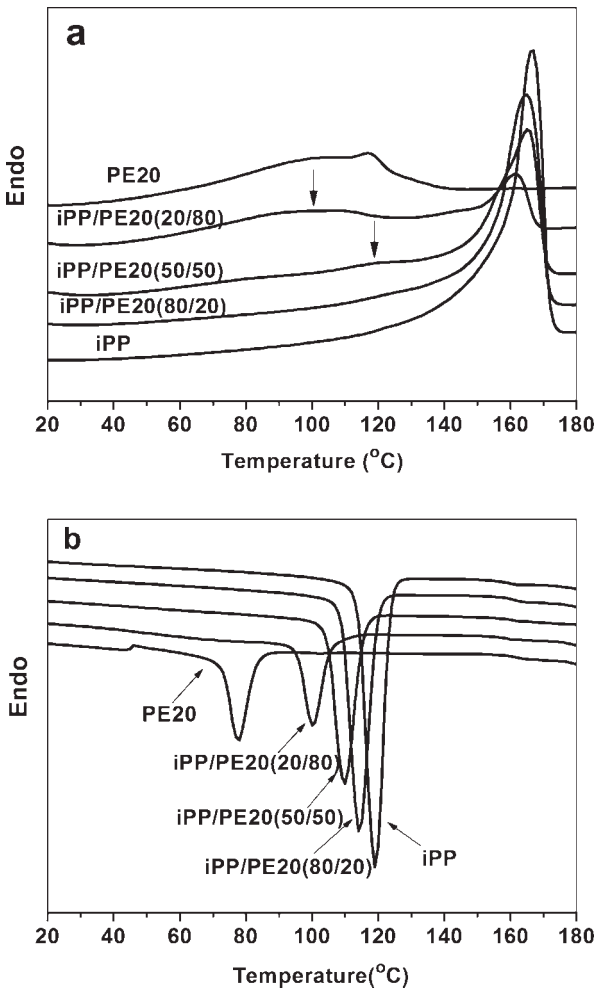

Figure 3 DSC curves of iPP blends with different PE20 content (wt %). (a) heating scans; (b) cooling scans.

Figure 3 shows the melting and crystallization behavior of iPP blends with the different PE20 content. And the corresponding melting and crystallization parameters obtained from the DSC curves are listed in Table III. The PE20 copolymer samples exhibit a broad melting peak with a melting temperature (T_m) of 117.0°C. With increasing the PE20 content, the melting peak of the iPP/PE20 blends shifts to the lower temperature. The melting temperature (T_m), the heat fusion of melting (ΔH_f), and crystallization temperature (T_c) of the iPP/PE20 blends decrease evidently with increasing PE20 contents. This is due to the fact that the PE20 copolymer with low ethylene-unit content has good compatibility with iPP.

It can be seen from Figure 3(b) that the crystallization temperatures of the iPP/PE20 blends are intermediate between those of iPP and PE20. The linear relationship between crystallization temperature and blend composition, as shown in Figure 4, indicates additive contributions of iPP and PE20 to the final crystallization temperature. The phenomena obtained from Figure 4 indicates that the crystallization ability and crystallization behavior of iPP have a strong function of PE20 content because the nucleation and growth rates of crystallization for iPP can be interfered with PE20 molecules. The thermal properties and crystallizations of iPP in the blends strongly depend on the miscibility between the iPP and PE20 component. In the iPP/PE20 blends, the PE20 copolymer chains having relatively low ethylene-unit content and high isotactic-propylene sequence is considered to be capable of participating in the crystallization process of iPP during solidification, resulting in that the PE20 molecular chains are incorporated partly in the crystal lattice and partly in the amorphous region. Therefore, the addition of PE20 can strongly affect the crystallization behavior of iPP.

Figure 5 shows the melting and crystallization behavior of iPP/PE23 blends with different weight ratios. And the corresponding melting and crystallization parameters obtained from the DSC curves are also listed in Table III. The PE23 copolymer has the higher ethylene-unit content than PE20. With the increase of the PE23 content, the melting peak of the blends does not change obviously, indicating that the addition of PE23 has no evident influence on the melting behavior of the iPP. The crystallization

TABLE III
The Crystallization and Melting Data of iPP in the iPP Blends with Different Copolymer Content from DSC

Samples	Weight ratio (%)	$\Delta H_{f,iPP}$ (J/g)	X_c of iPP (DSC)%	T_m (°C)	T_c (°C)
iPP	100	95	45.5	166.8	118.9
iPP/PE20	80/20	85	50.8	165.1	114.1
	50/50	53	50.7	165.4	109.8
	20/80	17	40.7	161.7	100.2
	0/100	–	–	117.0	77.6
iPP/PE23	80/20	79	47.2	165.7	115.8
	50/50	53	50.8	165.0	116.2
	20/80	21	50.2	165.4	111.5
	0/100	–	–	–	69.4

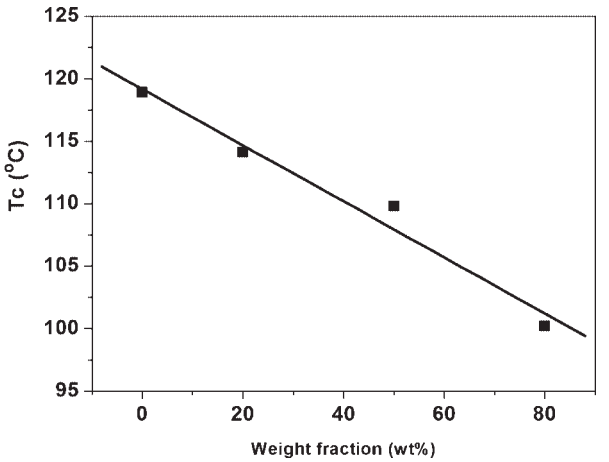

Figure 4 Effect of PE20 content on crystallization temperature of iPP.

temperature of the iPP/PE23 blends decreases with increasing the PE23 content. Comparing Figure 3 with Figure 5, it can be found that the PE20 molecules have more strong influence on the thermal behaviors of iPP than the PE23 molecules. This may be attributed to their difference in the ethylene-unit content. PE23 has the higher ethylene comonomer content and the weaker interaction with iPP. The domains of the PE23 copolymer could be separated with the iPP phase in the molten state prior to crystallization.[40] Therefore, the addition of PE23 has much weaker influence on the melting and crystallization behavior of iPP than that of PE20.

Isothermal crystallization behavior of iPP and its blends with PEc

The isothermal crystallization behavior and spherulite growth of iPP and iPP/PEc blends were investigated using a polarized optical microscope with a hot stage. Figures 6–8 show the evolution of the spherulite morphology with crystallization time for the iPP and its blends at T_c =130°C. Because the PE20 and PE23 copolymers have no ability to crystallize at 130°C, the micrographs of the blends represent the spherulite morphology of iPP component. With the addition of the copolymers, the spherulite growth of the iPP in the blends becomes slow, which may be due to the fact that the presence of the copolymers restricts the diffusion of the iPP chains during crystallization.

Figure 9 shows the time variation in the spherulite radius during isothermal crystallization at T_c = 130°C for all the blends and the pure iPP. It can be seen from the figures that the spherulite growth of all samples increases linearly with crystallization time. Therefore, the spherulite growth rates (G) of the pure iPP and the blends can be determined from the slope of the lines, and the calculated results are listed in Table IV. The larger is the slope of the line in Figure 9, the higher is the spherulite growth rate. The results obtained from Table IV show that the addition of the copolymers decreases the spherulite growth rates of iPP. It should be noted that spherulite growth rates (G) of the iPP/PE20 and iPP/PE22 blends are lower than those of the iPP/PE23 and iPP/PE24 blends, indicating the copolymers with lower ethylene-unit content have a greater effect on the crystallization process of iPP. On the other hand, the spherulite growth rates of the iPP/PE33 and iPP/PE34 blends are higher than those of the iPP/PE23 and iPP/PE24 blends, which illustrates that the copolymers with lower molecular weight have much weaker influence on the crystallization process of iPP. With the increase in the ethylene-unit content and the decrease in the molecular weight of the copolymers, the spherulite growth rates G of the blends is much closer to that of the pure iPP. The difference in the influence of the PEc copolymers

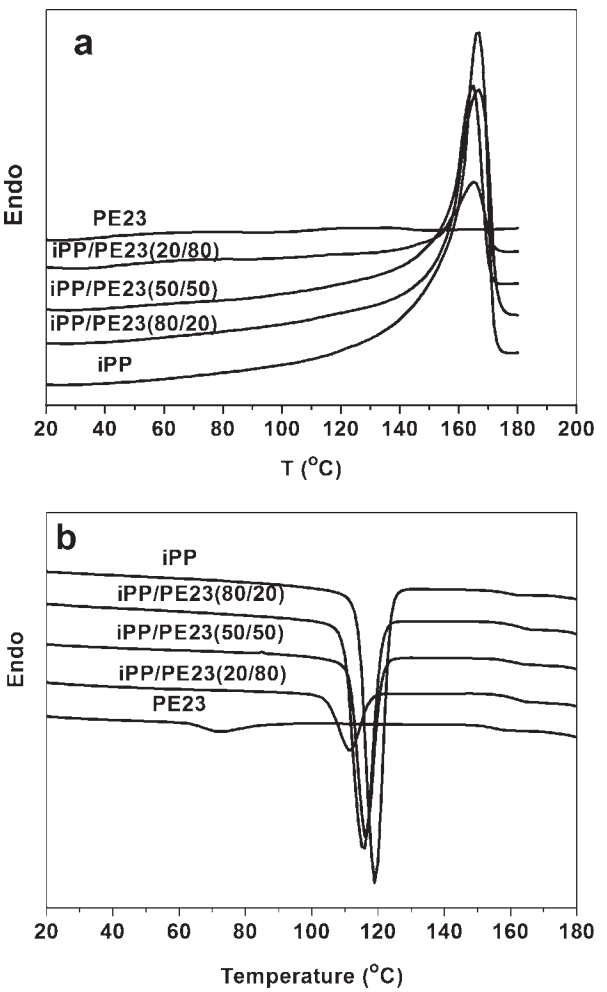

Figure 5 DSC thermograms iPP blends with different PE23 content (wt %). (a) heating scans; (b) cooling scans.

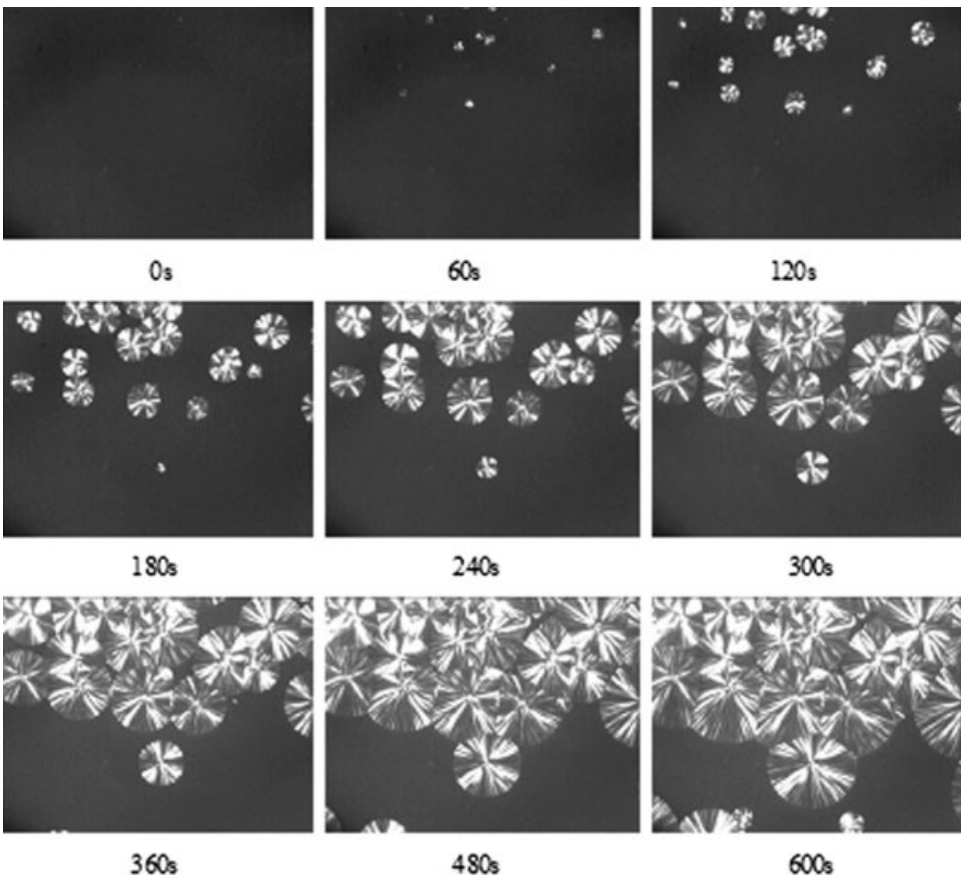

Figure 6 Polarized optical micrographs of iPP with various time at 403 K (×200).

with various ethylene-unit contents on the crystallization process of iPP may be related to the miscibility between iPP and the copolymers. In the iPP/PEc blends, the ssisotactic-propylene sequence in the PEc copolymer chains having relatively low ethylene-unit content such as PE20 and PE22 is considered to be capable of participating in the crystallization process of iPP during solidification, resulting in that the PEc copolymer chains are incorporated partly in the crystal lattice and partly in the amorphous region. Consequently, the increase in the content of PE20 copolymer for the iPP/PE20 blends can obviously decreases the spherulite growth rate of iPP, as seen in Figure 10.

On the other hand, spherulite growth rates G is almost closer to that of the pure iPP with decreasing the propylene-unit content of PEc copolymers for the iPP/PEc blends, indicating that the PE23, PE24, PE33, and PE34 copolymers have little effect on the crystallization process of iPP. This may be caused by the fact that the domains of these copolymers are separated with the iPP phase in the molten state prior to crystallization. These results can be proved by the fact that the spherulite growth rate G for the iPP/PE23 blends is independent of the PE23 fraction, as shown in Figure 11.

The spherulite growth rates of the pure iPP, the PP/PE20(80/20) and PP/PE23(80/20) blends at different crystallization temperature are shown in Table V. The spherulite growth rates of iPP and its blends reduce significantly with increasing the crystallization temperature. Compared to that of PP/PE23(80/20) blend, the spherulite growth rate of PP/PE20(80/20) blend reduces more obviously with increasing the crystallization temperature, which also indicates that the PE20 copolymer has more obvious influence on the crystallization behavior of iPP.

It is well known that Hoffman-Lauritzen secondary nucleation theory and its various modifications perhaps represent the most comprehensive and widely used methodology to interpret and model crystallization behavior of the polymers. According to this theory, the rate of nucleation is dependent on the crystallization temperature (degree of supercooling). The crystal growth process of the polymer is determined by two competing terms, diffusion-controlled at low crystallization temperatures, and nucleation-controlled at high crystallization temperatures. The isothermal spherulite growth rate G in the Hoffman-Lauritzen theory can be expressed by the following equation[53–55]:

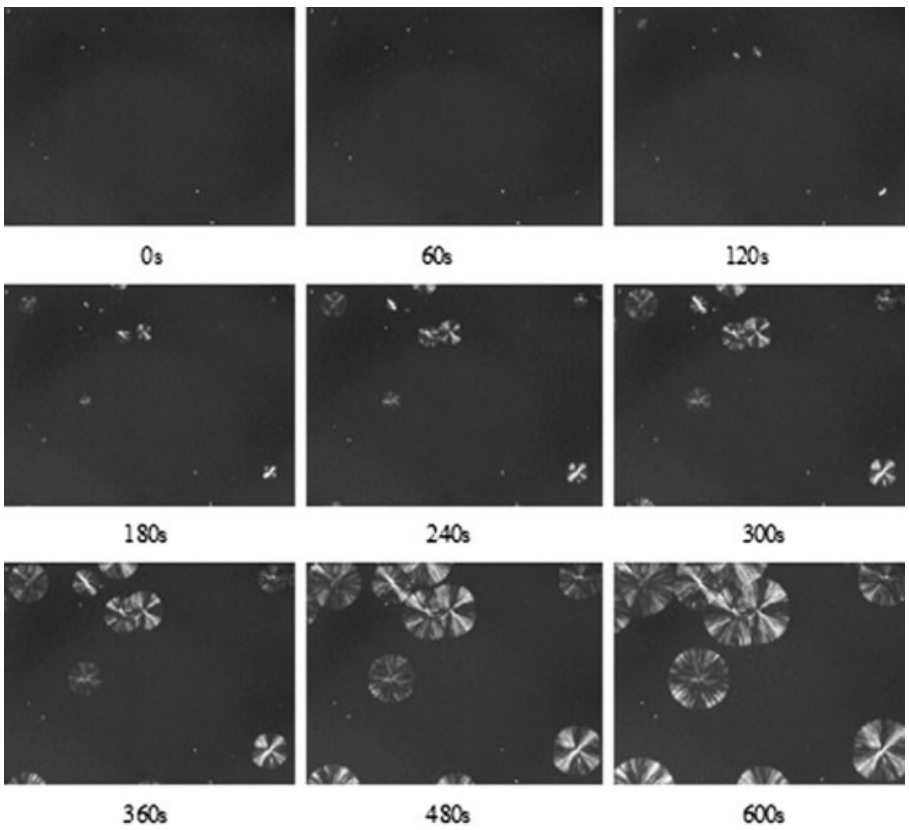

Figure 7 Polarized optical micrographs of iPP/PE20 (80/20) blends with various time at 403 K (×200).

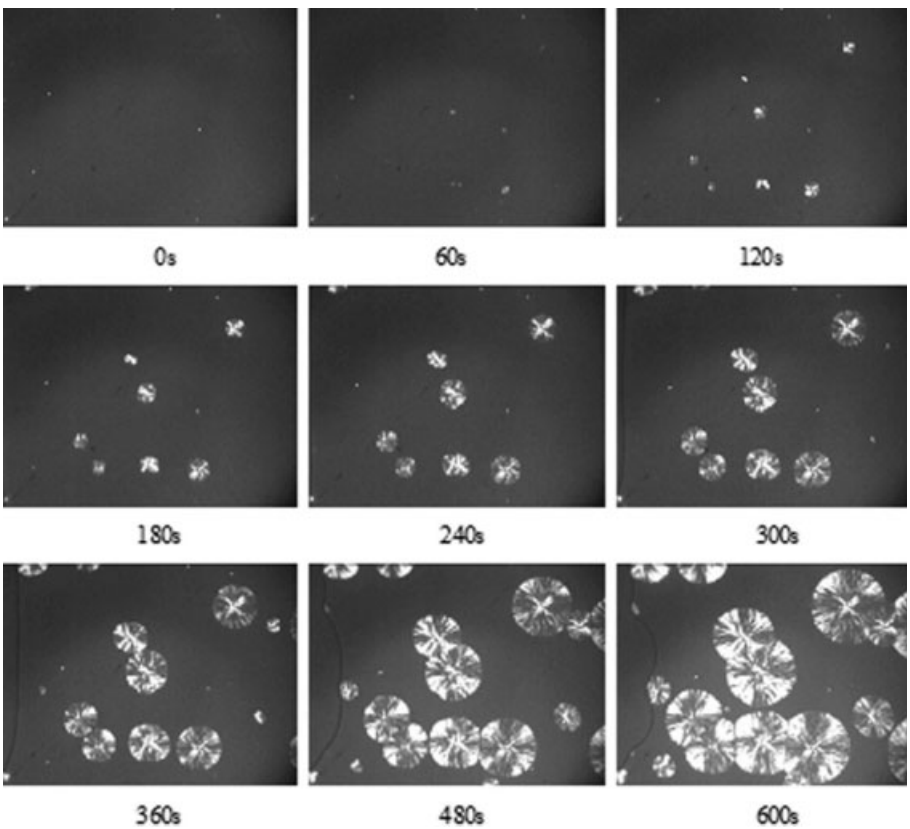

Figure 8 Polarized optical micrographs of iPP/PE23 (80/20) blends with various crystallization times at 403 K (×200).

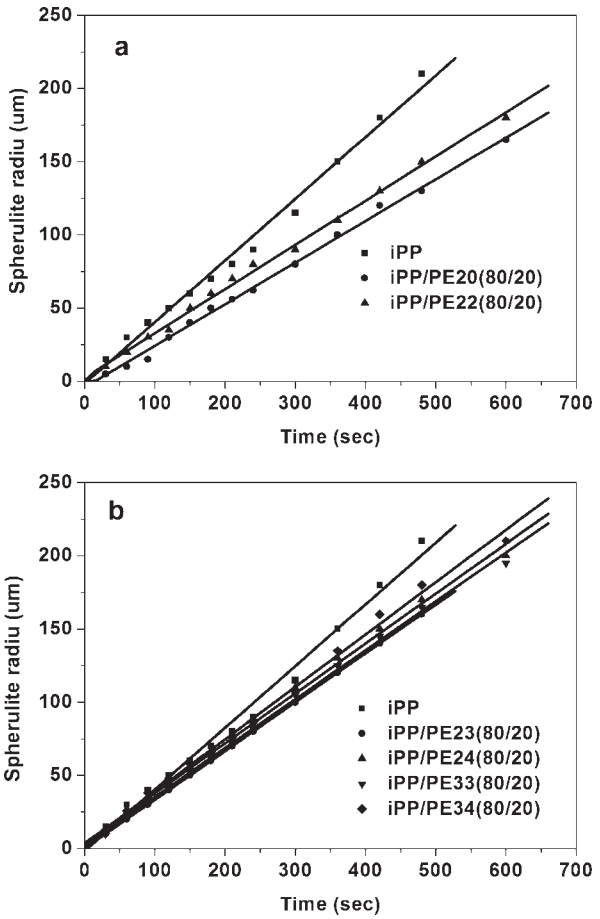

Figure 9 Spherulite radius versus time variation for iPP and iPP/PEc blends at 403 K.

$$G = G_0 \exp\left[-\frac{U^*}{R(T_c - T_\infty)}\right] \exp[-K_g/T_c(\Delta T)f] \quad (1)$$

where G is the observed linear growth rate, the front factor G_0 is the growth rate constant. The first factor, $\exp[-(U^*/R(T_c - T_\infty))]$, expresses the temperature dependence of the rate of transport for the crystallization segments, in which U^* is the activation energy required for polymer diffusion by reptation of crystallizing segments through the melt to the site

TABLE IV
Spherulite Growth Rate of iPP and iPP/PEc Blends at 403 K

Sample	G (μm/s)
iPP	0.421
iPP/PE20(80/20)	0.284
iPP/PE22(80/20)	0.300
iPP/PE23(80/20)	0.333
iPP/PE24(80/20)	0.341
iPP/PE33(80/20)	0.345
iPP/PE34(80/20)	0.358

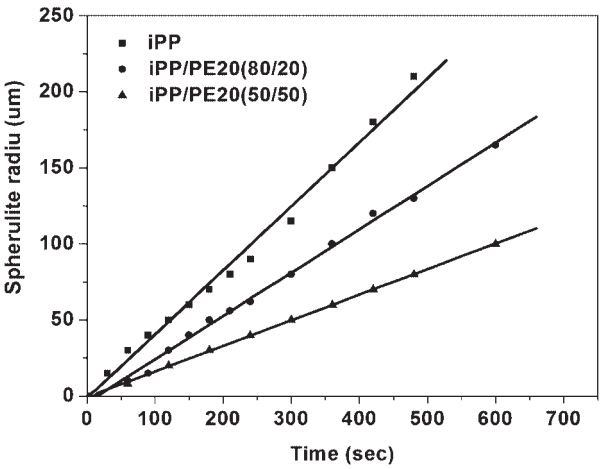

Figure 10 Spherulite radius versus time variation for iPP and iPP/PE20 blends at 403 K.

of crystallization, the value of U^* as described in this study is 6280 J/mol for the pure iPP and the iPP/PEc blends.[56,57] The second factor, $\exp[-K_g/T_c(\Delta T)f]$, expresses the temperature dependence of the nucleation rate. R is the universal gas constant. T_c is the crystallization temperature (K), $T_\infty = T_g - 30$ (K), T_g is the glass transition temperature (K), in this study, $T_\infty = 231.2$ K for the pure iPP.[55] $\Delta T = (T_m^0 - T_c)$ is the degree of supercooling (K), T_m^0 is the equilibrium melting temperature of lamellae with infinite thickness (K), which is 458 K for iPP reported by Mezghani et al.[56] In this study, we assumed that T_m^0 of the iPP blends is identical with that of the pure iPP because there is no specific interaction between the components, which affects the equilibrium melting temperature. f Is a correction factor for the change of the heat of fusion at high supercoolings, $f = 2T_c/(T_m^0 + T_c)$.

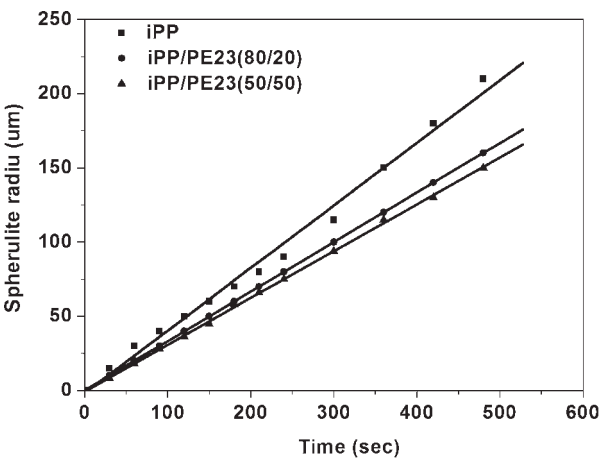

Figure 11 Spherulite radius versus time variation for iPP and iPP/PE23 blends at 403 K.

TABLE V
Spherulite Growth Rates of iPP, iPP/PE20, and iPP/PE23 Blends at Different Crystallization Temperature

Sample	Temperature (°C)	G (μm/s)
iPP	125	0.758
	130	0.421
	135	0.234
iPP/PE20(80/20) blend	125	0.642
	130	0.284
	135	0.126
iPP/PE23(80/20) blend	125	0.649
	130	0.333
	135	0.172

For the purpose of the better understanding of nucleation kinetics, the spherulite growth rates of the iPP/PE20 and iPP/PE23 blends are analyzed on the basis of the polymer-dilutent theory proposed by Boon and Azcue.[58] The spherulite growth rate G for the iPP blends can be described by the following corrected equation:

$$\ln G - \ln \varphi_2 + \left[\frac{U^*}{R(T_c - T_\infty)}\right] - \frac{0.2T_m^0 \ln \varphi_2}{\Delta T} = \ln G_0 - \frac{K_g}{T_c(\Delta T)f} \quad (2)$$

where φ_2 is the volume fraction of the crystallizable component, K_g is a nucleation parameter in dependent of the crystallization temperature. The crystallization regime analysis for the pure iPP, the iPP/PE20, and iPP/PE23 blends are shown in Figure 12. Apparently, the plot of $\{\ln G - \ln \varphi_2 + [U^*/R(T_c - T_\infty)] - (0.2T_m^0 \ln \varphi_2/\Delta T)\}$ vs. $[1/T_c(\Delta T)f]$ shows a single straight line, indicating that there is no regime transition for the iPP and its blends. The nucleation constant K_g in eq. (2) can be determined from the slope of the lines in Figure 12 and defined as:

$$K_g = \frac{2b_0 \sigma \sigma_e T_m^0}{k(\Delta h_f).} \quad (3)$$

where b_0 is the thickness of the chain stem, which is $b_0 = 6.26$ Å[55] for iPP assuming crystal growth only on the (110) plane, σ is the lateral surface free energy, σ_e is the fold surface free energy, k is the Boltzmann constant (1.38053×10^{-23} J/K), and Δh_f is the heat of fusion per unit volume (196 MJ/m^3 for iPP).[56] The lateral surface free energy can be calculated from the Hoffman modification of Thomas-Stavely equation as following:

$$\sigma = 0.1\Delta h_f (a_0 b_0)^{1/2} \quad (4)$$

where a_0 is the width of the chain stem, which is $a_0 = 5.49$ Å[55] for iPP. Furthermore, the value of σ is constant in all crystallization regimes. Hoffman and Clark determined the magnitude of σ to be 11.5×10^{-3} J/m^2 for iPP using eq. (4). In the present work, we calculated the value of σ_e using eq. (3) and $\sigma = 11.5 \times 10^{-3}$ J/m^2.[55] The calculated value of crystallization kinetic parameters: K_g, σ_e are listed in Table VI. For the pure iPP, the value of K_g is 2.0×10^5 (K^2), which is comparable with the reported value.[59] From the results listed in Table VI, it can be observed that the values of K_g and σ_e for the iPP/PE20 blends are higher than that of the pure iPP, indicating that the addition of the PE20 decreases the nucleation rate and improves the fold surface free energy for iPP, which further affects obviously the crystallization process of the iPP. On the other hand, the values of K_g and σ_e for the iPP/PE23 blends are comparable with that for the iPP, which implies the addition of the PE23 copolymer has little effect on the crystallization process of iPP. These results are consistent with the previous DSC and PLM results.

To be universally known, the crystallization process of polymers is controlled by primary nucleation and crystal growth (secondary nucleation). Primary nucleation is the process by which molten polymer chains become aligned to form nuclei when the polymer melt is cooled down below its equilibrium melting temperature. Secondary nucleation is defined as a surface nucleation on an existing crystal nuclei growth plane, which is responsible for further growth of the activated nucleus.[60] Generally, the EPR rubbers showing little crystallizability are essentially immiscible with iPP.[43] In the present work, with increasing the ethylene-unit content for the PEc copolymers, the length and number of crystallizable

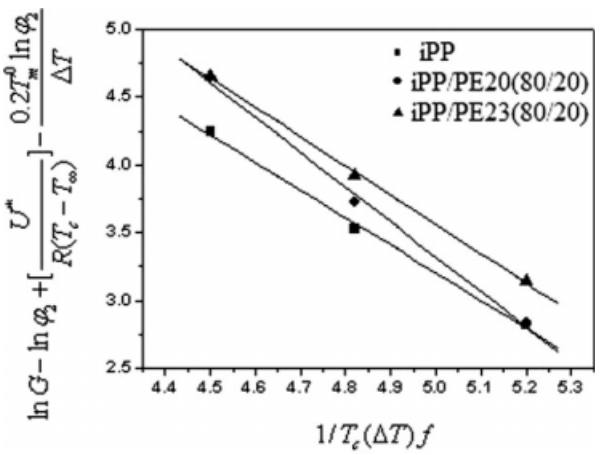

Figure 12 Relationship between $\ln G - \ln \varphi_2 + [U^*/R(T_c - T_\infty)] - 0.2T_m^0 \ln \varphi_2/\Delta T$ and $1/T_c(\Delta T)f$ for iPP, iPP/PE20, and iPP/PE23 blend at different crystallization temperature.

TABLE VI
Values of Parameters Determined from Kinetic Analysis Plots for iPP and Its Blends

Sample	G_0 (m/s)	$Kg \times 10^{-5}$ (K^2)	$\sigma\sigma_e$ ($\times 10^{-4}$ J/m^2)	σ ($\times 10^{-3}$ J/m^2)	σ_e ($\times 10^{-3}$ J/m^2)
iPP	13.4	2.0	9.6	11.5	83.6
iPP/PE20(80/20)	16.2	2.6	12.2	11.5	105.9
iPP/PE23(80/20)	14.4	2.1	10.2	11.5	88.7

sequences obviously decrease. The PE20 copolymer with high propylene-unit content has the better miscible with the iPP than the PE23 copolymer with higher ethylene comonomer concentration. This difference in the miscibility will have serious influence on the crystallization process of the corresponding blends with iPP. As described in the previous section, the PE20 copolymer, acting as a dilution agent, can be considered to be capable of participating in the crystallization process of iPP. The PE20 chain portions that are not available to participate in the crystallization process are trapped into the interlamellar region. Thus, the existence of PE20 molecules in the amorphous region between the neighbor lamellae will spread the interlamellar distance and increase the amorphous layer thickness, leading to the enhancement of the mobility of the crystallizable iPP chains and to the reduction of the number of tie molecules operating as obstacles for transportation motion or reptation of crystallizable chains. Therefore, the addition of the PE20 copolymer restricts the spherulite growth of the iPP and decreases the nucleation rate. On the other hand, the domains of PE23 copolymer are separated with the iPP phase in the molten state prior to crystallization due to the poor miscibility between iPP and PE23 copolymer with high ethylene-unit content. Therefore, the PE23 copolymer has little influence on the crystallization process of iPP.

CONCLUSIONS

In the present work, the isothermal crystallization behavior and melting behavior of iPP blends with PEc copolymers were investigated. The addition of PEc copolymers decreases the crystallization temperature of iPP. PLM results show that the spherulite radii increases linearly with crystallization time for all the samples. The spherulite growth rate of the iPP/PE20 blends decreases with increasing the PE20 content.

The difference in the miscibility of iPP/PE20 and iPP/PE23 blends has different influence on the thermal and crystallization behaviors of the blends. With the increase in the ethylene-unit content of the PEc copolymers, the effect of the copolymers on the crystallization behavior of iPP becomes weaker. The crystallizable sequences in the PE20 copolymer with the lower ethylene-unit content can participate in the crystallization process of iPP, resulting in that the PEc copolymer chains are incorporated partly in the crystal lattice, partly in the amorphous region, and finally influencing the crystallization process of iPP. The addition of the PE20 copolymer increases the nucleation rate constant (K_g) and the fold surface energy (σ_e) of iPP and further decreases the overall crystallization rate of iPP. For the PE23 copolymer with the higher ethylene-unit content, the copolymers had no ability to participate in crystallization process. The domains of the copolymers are separated with the iPP phase in the molten state prior to crystallization. Therefore, the PE23 copolymer has little influence on the crystallization process of iPP.

References

1. Gibon, C. M.; Norvez, S.; Girault, S. T.; Goldbach, J. T. Macromolecules 2008, 41, 5744.
2. Cui, L. M.; Zhang, Y.; Zhang, Y. X. J Polym Sci Part B: Polym Phys 2006, 44, 3288.
3. Hu, Y. S.; Kamdar, A. R.; Ansems, P.; Chum, S. P.; Hiltner, A.; Baer, E. Polymer 2006, 47, 6387.
4. Wang, Z. G.; Phillips, R. A.; Hsiao, B. S. J Polym Sci Polym Phys Ed 2000, 38, 2580.
5. Phillips, R. A. J Polym Sci Polym Phys Ed 2000, 38, 1947.
6. Wang, Z. G.; Phillips, R. A.; Hsiao, B. S. J Polym Sci Polym Phys Ed 2001, 39, 1876.
7. Foresta, S.; Piccarolo, G.; Goldbeck, W. Polymer 2001, 42, 1167.
8. Silvestri, R.; Sgarzi, P. Polymer 1998, 39, 5871.
9. Phillips, R. A.; Jones, R. L. Macromol Chem Phys 1999, 200, 1912.
10. Li, J.; Shanks, R. A.; Long, Y. J Appl Polym Sci 2001, 82, 628.
11. Weiss, R. A.; Sen, A.; Pottick, L. A.; Willis, C. L. Polymer 1991, 32, 1867.
12. Weiss, R. A.; Sen, A.; Pottick, L. A.; Willis, C. L. Polymer 1991, 32, 2785.
13. Qiao, J.; Hamaya, T.; Okada, T. Polymer 2005, 46, 10809.
14. Karger, K. J.; Czigany, T. Compos Part A: Appl Sci Manuf 1998, 29, 1319.
15. López-Manchado, M. A.; Arroyo, M. Polymer 2000, 41, 7761.
16. Stocker, W.; Schumacher, M.; Graff, S. Macromolecules 1998, 31, 807.
17. Huo, H.; Jiang, S. C.; An, L. J. Macromolecules 2004, 37, 2478.
18. Yamamoto, Y.; Inoue, Y.; Onai, T. Macromolecules 2007, 40, 2745.
19. Masubuchi, Y.; Watanabe, K.; Nagatake, W.; Takimoto, J. I.; Koyama, K. Polymer 2001, 42, 5023.
20. Nieh, J. Y.; Lee, L. J. Polym Eng Sci 1998, 38, 1121.
21. Pogodina, N. V.; Lavrenko, V. P.; Srinivas, S.; Winter, H. H. Polymer 2001, 42, 9031.

22. Koscher, E.; Fulchiron, R. Polymer 2002, 43, 6931.
23. Devaux, N.; Monasse, B.; Haudin, J. M.; Moldenaers, P.; Vermant, J. Rheol Acta 2004, 43, 212.
24. Kyu, T.; Vadhar, P. J Appl Polym Sci 1986, 32, 5575.
25. Tashiro, K.; Satkowski, M. M.; Stein, R. S.; Li, Y.; Chu, B.; Hsu, S. L. Macromolecules 1992, 25, 1809.
26. Schuman, T.; Stepanov, E. V.; Nazarenko, S.; Capaccio, G.; Hiltner, A.; Baer, E. Macromolecules 1998, 31, 4551.
27. Alamo, R. G.; Glaser, R. H.; Mandelkern, L. J Polym Sci Part B: Polym Phys 1988, 26, 2169.
28. Kim, M.-H.; Alamo, R. G.; Lin, J. S. Polym Eng Sci 1999, 39, 2117.
29. D'Orazio, L.; Mancarella, C.; Martuscelli, E. Polymer 1991, 32, 1186.
30. D'Orazio, L.; Mancarella, C.; Martuscelli, E. J Mater Sci 1991, 26, 4033.
31. D'Orazio, L.; Mancarella, C.; Martuscelli, E. Polymer 1993, 34, 3671.
32. D'Orazio, L.; Mancarella, C.; Martuscelli, E. J Appl Polym Sci 1994, 53, 387.
33. Da Silva, A. L. N.; Tavares, M. I. B.; Politano, D. P.; Coutinho, F. M. B.; Rocha, M. C. G. J Appl Polym Sci 1997, 66, 2005.
34. Da Silva, A. L. N.; Rocha, M. C. G.; Coutinho, F. M. B.; Bretas, R.; Scuracchio, C. J Appl Polym Sci 2000, 75, 692.
35. Kukaleva, N.; Jollands, M.; Cser, F.; Kosior, E. J Appl Polym Sci 2000, 76, 1011.
36. Kukaleva, N.; Cser, F.; Jollands, M.; Kosior, E. J Appl Polym Sci 2000, 77, 1591.
37. Dharmarajan, N. R.; Yu, T. C. Plast Eng 1996, 52, 33.
38. Yu, T. C. Polym Eng Sci 2001, 41, 656.
39. McNally, T.; McShane, P.; Nally, G. M.; Murphy, W. R.; Cook, M.; Miller, A. Polymer 2002, 43, 3785.
40. Nitta, K.-H.; Shin, Y.-W.; Hashiguchi, H.; Tanimoto, S.; Terano, M. Polymer 2005, 45, 965.
41. Yamaguchi, M.; Miyata, H.; Nitta, K. J Polym Sci Part B: Polym Phys 1997, 35, 953.
42. Yamaguchi, M.; Nitta, K.; Miyata, H.; Masuda, T. J Appl Polym Sci 1997, 63, 46.
43. Yamaguchi, M.; Miyata, H.; Nitta, K. J Appl Polym Sci 1996, 62, 87.
44. Lim, S. W.; Lee, K. H.; Lee, C. H. Polymer 1999, 40, 2837.
45. Coppola, F.; Greco, R.; Martuscelli, E. Polymer 1988, 29, 963.
46. Wenig, W.; Asresahegn, M. Polym Eng Sci 1993, 33, 877.
47. Zhang, X. Q.; Zhao, Y.; Wang, Z. G.; Zheng, C. X.; Su, Z. Q.; Sun, P. Y.; Wang, D. J.; Han, C. C.; Xu, D. F. Polymer 2005, 46, 5956.
48. Seki, M.; Nakano, H.; Yamauchi, S.; Suzuki, J.; Matsushita, Y. Macromolucules 1999, 32, 3227.
49. Cham, P. M.; Lee, T. H.; Marand, H. Macromolecules 1994, 27, 4263.
50. Chen, J. H.; Tsai, F. C.; Nien, Y. H.; Yeh, P. H. Polymer 2005, 46, 5680.
51. Keith, H. D.; Padden, F. J. J Appl Phys 1964, 35, 1270.
52. Keith, H. D.; Padden, F. J. J Appl Phys 1964, 35, 1286.
53. Hoffman, J. D.; Miller, R. L. Polymer 1997, 38, 1351.
54. Hoffman, J. D. Polymer 1983, 34, 3.
55. Clark, E. J.; Hoffman, J. D. Macromolecules 1984, 17, 878.
56. Assoulineb, E.; Pohl, S.; Fulchion, R.; Gerard, J. F., et al. Polymer 2000, 41, 7843.
57. Janimak, J. J.; Cheng, S. Z. D.; Giusti, P. A.; Hsieh, E. T. Macromolecules 1991, 24, 2253.
58. Boon, J.; Azcue, J. M. J Polym Sci 1968, 6, 885.
59. Di Lorenzo, M. L.; Cimmino, S.; Silvestre, C. Macromolecules 2000, 33, 3828.
60. Raimo, M. Prog Polym Sci 2007, 32, 597.